Above-threshold ionization of atoms irradiated by sinusoidally phase-modulated pulses

Haiying Yuan,[1,2] Yujun Yang,[1,*] Fuming Guo,[1] Jigen Chen,[3] Jun Wang,[1] and Zhiwen Cui[2,†]
[1]*Institute of Atomic and Molecular Physics, Jilin University, Changchun 130012, China*
[2]*College of Physics, Jilin University, Changchun 130012, China*
[3]*Zhejiang Provincial Key Laboratory for Cutting Tools, Taizhou University, Jiaojiang 318000, Zhejiang, China*

(Received 8 June 2023; revised 3 December 2023; accepted 10 January 2024; published 5 February 2024)

By solving the time-dependent Schrödinger equation in momentum space, the photoelectron emission from atoms under the irradiation of 400 nm sinusoidal phase-modulated shaped pulses was investigated. It was found that by controlling the phase and amplitude of the pulses in the frequency domain, in addition to the photoelectron peaks generated by the interference of multiple-cycle ionization, additional resonant peak structures and interference phenomena can be observed in the photoelectron emission spectrum. Through the analysis of photoelectrons from different subpulses within the shaped pulse, it was discovered that these structures arise from the modulation of ionization and excitation processes by multiple subpulses within the shaped pulse. This study demonstrates the significant importance of utilizing shaped pulses for the control of photoelectron emission.

DOI: 10.1103/PhysRevA.109.023104

I. INTRODUCTION

With the continuous development of laser technology, the interaction of ultrastrong and ultrashort laser pulses with atoms, molecules, and solids has produced many new physical phenomena, such as above-threshold ionization (ATI), nonsequential double ionization, and high-order-harmonic generation (HHG) [1–12]. Above-threshold ionization refers to the process where the total energy absorbed by the emitted electrons during ionization exceeds the required ionization energy [13]. Since photoelectron emission is sensitive to the parameters of the driving laser pulse and the state of atoms and molecules, photoelectron emission spectroscopy can be used in experiments to measure the carrier-envelope phase (CEP) of the driving laser [14,15] and probe the internal structure of atoms and molecules [16]. The study of above-threshold ionization provides a powerful technical tool for detecting and controlling the ultrafast dynamics of matter.

From the frequency-domain perspective, above-threshold ionization can be understood as a process of multiphoton transition, in which electrons absorb energy from multiple photons and transition to the continuum state for ionization. The spacing between adjacent peaks in the photoelectron emission spectra corresponds to the energy of a single photon, i.e., $\hbar\omega_0$, where ω_0 is the central frequency of the incident laser pulse. Under the action of a strong laser field, the energy levels of the atom are shifted and the energy position of the photoelectron peak can be given by the formula $E_k = n\omega_0 - I_p - U_p$ (where I_P is the ionization potential of the atom, U_P is the ponderomotive energy of the electron in the laser field, $U_P = E_0^2/4\omega_0^2$, and E_0 is the peak amplitude of the incident laser field) [17].

In the photoelectron emission spectrum, in addition to the ATI peaks generated by the interference of emitted electrons of different laser pulse cycles, many small photoelectron peaks can also be observed under certain conditions. The reasons for the generation of these small photoelectron peaks may originate from different physical mechanisms, most typically in two cases. The first one is the interference of ionized electron wave packets induced by the dynamic Stark effect during the rising and falling edges of the laser pulse [18–20]. The second one occurs at higher laser intensities, where significant energy shifts in excited states result in resonant ionization when the photon energy matches the energy required for electronic transitions from the ground state to the excited state, which is known as Freeman resonance [21]. The photoelectron emission spectrum has been studied in depth both theoretically and experimentally for many years. However, it is not an easy task to significantly enhance ionization and control the interference of wave packets by adjusting the excited state.

Shaping pulses are suitable laser electric fields to achieve these quantum controls. The shaping pulse can control the excited state with high efficiency so that the excited state can be distributed, resulting in increased ionization, and also provides more convenience for changing optoelectronic interference. By changing the amplitude, phase, and polarization of laser pulses in the frequency domain, almost arbitrarily shaped pulses can be obtained in the time domain [22,23]. Präkelt *et al.* used shaping laser pulses to study in detail the phase effect on quantum control experiments of two-photon transitions of sodium atoms from 3*s* to 4*s* [24]. Wollenhaupt *et al.* applied femtosecond shaping laser pulses to realize quantum control of potassium atom ionization and discussed the excitation and ionization process induced by shaping pulses [25]. Lahiri *et al*. enhanced the two-photon excitation fluorescence of the fluorescent Schiff photobase (E)-7-((butylimino)methyl)-*N,N*-diethyl-9,9-dimethyl-

*yangyj@jlu.edu.cn
†cuizw@jlu.edu.cn

9*H*-fluoren-2-amine (FR0-SB) in methanol by a factor of 1.75 by controlling the quantum interference between the two optical excitation paths using femtosecond shaping laser pulses [26]. Li *et al.* proved that shaping laser pulses can control the electron dynamics and nuclear dynamics of the ion yield [27].

Our previous work investigated the photoelectron emission spectrum under the action of 800 nm sinusoidal phase-modulation pulses, focusing on the analysis of the photoelectron emission spectrum caused by the short-period interpulse interference, and we explained the reason for the obvious subpeak structure on the photoelectron emission spectrum. However, no clear resonance phenomenon was observed [28]. This study was limited to a relatively small range of laser intensity, and only the action of a single main pulse with a short period was considered, while there was a lack of in-depth studies on the combined effect of multiple pulses with a long period. To address this issue, we chose 400 nm sinusoidal phase-modulation shaping laser pulses and investigated the effects of shaping multiple pulses with long periods on atomic excitation and ATI by varying the electric-field peak amplitude of the shaping laser pulses. It was found that in addition to the appearance of photoelectron peaks and sideband peaks generated by the pulse width effect in the photoelectron emission spectrum, resonance peaks with higher intensities than those from Fourier-limit laser pulses with the same laser parameters can also be observed. These resonance peaks originate from the different laser subpulses modulating the excited states, thereby enhancing ionization. At the same time, it was also proved that there are many subpeaks in the photoelectron emission spectrum from sinusoidally phase-modulated pulses, which arise from the interference of ionized electrons from different subpulses. By phase-modulating laser pulses, Freeman resonance and photoelectron interference can be observed simultaneously and affect the photoelectron emission spectrum.

II. SCHEME AND THEORETICAL METHOD

In order to obtain the photoelectron emission spectrum of atoms under the action of shaping laser pulses, it is necessary to numerically solve the time-dependent Schrödinger equation (TDSE) of atoms under the action of a laser field. The numerical solution of this equation is usually calculated based on the coordinate space, but for multiple cycles of an intense laser action, ionized electrons will move to the region away from the parent ion. To obtain an accurate electron wave function, many grid points are required in the calculation, which makes it very difficult to calculate accurately in the coordinate space. However, since the momentum of ionized electrons is finite in any process, as long as an appropriately large momentum boundary is set in the momentum space, the electron wave function can be calculated without boundary reflection and there will be obvious advantages in the momentum-space calculation. Based on the momentum space, this paper uses the generalized time-dependent pseudospectral method to solve the TDSE of the system, which reduces the requirements for computing resources [29–31]. Under the dipole approximation and velocity specification, the time-dependent Schrödinger equation satisfied by atoms is (atomic units are used throughout this paper, unless specified otherwise)

$$i\frac{\partial}{\partial t}\psi(\mathbf{r},t)=\left[\frac{\hat{\mathbf{p}}^2}{2}+\frac{1}{c}\mathbf{A}(t)\hat{\mathbf{p}}+U(\mathbf{r})\right]\psi(\mathbf{r},t), \tag{1}$$

where c is the speed of light, and $U(\mathbf{r})$ represents the Coulomb potential of the atom for the hydrogen atom $U(\mathbf{r})=-\frac{1}{r}$. $\mathbf{A}(t)$ denotes the vector potential of the laser pulse and $\widehat{\mathbf{p}}$ stands for the dynamic momentum.

The electric-field form of the laser pulse used before shaping this paper is

$$E(t)=E_0 f(t)\sin(\omega_0 t+\phi), \tag{2}$$

where the linear polarization laser pulse along the Z axis in the direction of the laser electric field is selected, the peak electric amplitude of the laser pulse is $E_0=0.09$ a.u. (light intensity $I=2.84\times10^{14}$ W/cm^2), the center frequency of the laser pulse is $\omega_0=0.114$, $\phi=0$ is the carrier-envelope phase (CEP) of the laser pulse, where $f(t)$ is the pulse envelope function, $f(t)=e^{\frac{-4\ln 2(t-\tau_c)^2}{\tau_p{}^2}}$, τ_c is the center of the envelope, and τ_p is the full width at half maximum (FWHM) of the laser pulse before shaping with 31.2 fs [about 23 optical cycles, o.c.].

The momentum-space wave function $\Phi(\mathbf{p},t)$ can be obtained by the Fourier transform of the wave function of the coordinate space $\Psi(\mathbf{r},\mathbf{t})$,

$$\Phi(\mathbf{p},t)=\frac{1}{(2\pi)^{3/2}}\int\Psi(\mathbf{r},t)\exp(-i\mathbf{p}\cdot r)d\mathbf{r}. \tag{3}$$

Substituting Eq. (3) into Eq. (1), we can obtain the time-dependent Schrödinger equation for the momentum space,

$$i\frac{\partial}{\partial t}\Phi(\mathbf{p},t)=\left[\frac{\mathbf{p}^2}{2}+\frac{1}{c}\mathbf{A}(t)\cdot\mathbf{p}\right]\Phi(\mathbf{p},t)+\int V(\mathbf{p},\mathbf{p}')\Phi(\mathbf{p}',t)d\mathbf{p}'. \tag{4}$$

Here, $V(\mathbf{p},\mathbf{p}')$ is the Coulomb potential of the momentum space,

$$V(\mathbf{p},\mathbf{p}')=\frac{1}{(2\pi)^3}\int U(\mathbf{r})\exp[i(\mathbf{p}'-\mathbf{p})\cdot\mathbf{r}]d\mathbf{r}. \tag{5}$$

The partial waves expression for the momentum-space Coulomb potential is

$$V(\mathbf{p},\mathbf{p}')=\frac{1}{pp'}\sum_{l=0}^{l_{\max}}\sum_{m=-l}^{l}V_l(p,p')Y_{lm}(\theta,\phi)Y_{lm}^*(\theta',\phi'), \tag{6}$$

where $p=|\mathbf{p}|$ and

$$V_l(p,p')=-\frac{Z}{\pi}Q_l\left(\frac{p^2+p'^2}{2pp'}\right). \tag{7}$$

Here, $Q_l(z)$ is the second type of Legendre function.

The wave function $\Phi(\mathbf{p},t)$ can be expanded in the partial waves as [32–34]

$$\Phi(\mathbf{p},t)=\frac{1}{p}\sum_{l=0}^{l_{\max}}\varphi_l(p,t)Y_{l0}(\theta,\phi), \tag{8}$$

where $l_{\max}$ is the maximum number of partial waves, $\varphi_l(p,t)$ is the radial wave function, and $Y_{l0}(\theta,\varphi)$ is the spherical harmonic function.

By substituting Eqs. (6) and (8) into Eq. (4), we obtain the integral differential equation for the radial wave function $\varphi_l(p,t)$ in the momentum space as

$$i\frac{\partial}{\partial t}\varphi_l(p,t) = \frac{p^2}{2}\varphi_l(p,t) + \int V_l(p,p')\varphi_l(p',t)dp' + \frac{1}{c}pA(t)[\alpha_{l+1}\varphi_{l+1}(p,t) + \alpha_l\varphi_{l-1}(p,t)], \quad (9)$$

where $\alpha_l = \frac{l}{\sqrt{(2l-1)(2l+1)}}$.

Since the second kind of Legendre function has a logarithmic singularity at $p = p'$, the momentum-space Coulomb potential $V_l(p,p')$ has a logarithmic singularity at $p = p'$ in the partial wave function. Therefore, this singularity presents a difficulty in solving the time-dependent Schrödinger equation in the momentum space. To remove this singularity, the Legendre method is employed [35].

Since the momentum of the electron is finite, the electron wave function in the momentum space can be set to a value of 0 outside a sufficiently large boundary $p_{\max}$ and the computational space can be chosen to be $p \in [0, p_{\max}]$. To solve Eq. (9) numerically, we used the pseudospectral method for the momentum-space calculation. We first mapped the momentum-space region $p \in [0, p_{\max}]$ to a new region $x \in [-1, 1]$, and the corresponding mapping function is

$$p(x) = \gamma\frac{1+x}{1-x+x_m}, \quad (10)$$

where γ is the mapping parameter, $x_m = 2\gamma/p_{\max}$, and the smaller the value of γ, the smaller the momentum p when the number of lattice points will be more; according to the different physical processes of the calculation, one can choose different mapping parameters, adjust the number of dots, and improve the accuracy of the calculation of the wave function. The solution of Eq. (4) using a generalized time-dependent pseudospectral scheme gives the time-dependent wave function of the system. Since a linearly polarized laser pulse with the initial state of $1s$ is used, the equation of the scattering state is given by

$$\Psi^-(\boldsymbol{k},\boldsymbol{p}) = \sqrt{\frac{2}{\pi}}\sum_{l=0}^{\infty} i^l \exp(-i\delta_l)\psi_{kl}(p)Y_{l0}^*(\hat{\boldsymbol{p}})Y_{l0}(\hat{\boldsymbol{k}}), \quad (11)$$

where $\hat{\boldsymbol{p}}$ and $\hat{\boldsymbol{k}}$ represent the unit vectors in the direction of $\boldsymbol{p}$ and $\boldsymbol{k}$, respectively, $\varepsilon = \frac{k^2}{2}$, $\psi_{kl}(p)$ are eigenfunctions with no laser field, and δ_l is the scattering phase shift.

In the calculation in this paper, the grid number in p is 2000 and the angular momentum number is 25. The corresponding single differential scattering cross section is calculated by projecting the scattering continuum to the wave function of the system at the end of the laser,

$$\frac{dP_\varepsilon}{d\varepsilon} = \sum_l |b_l(\varepsilon, t_{fin})|^2, \quad (12)$$

where $b_l(\varepsilon,t)$ is the continuous state population amplitude of the energy normalized for different partial waves, and t_{fin} is the end moment of the laser.

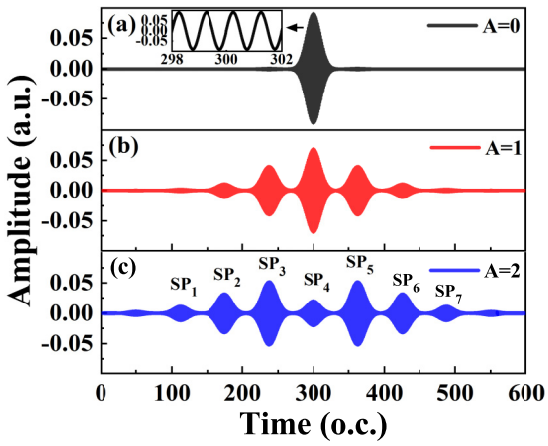

FIG. 1. Sinusoidally phase-modulated laser pulses at different shaping parameters A: (a) $A = 0$, (b) $A = 1$, and (c) $A = 2$.

In order to obtain ionization information, the bound state wave function of the system is projected onto the total wave function to obtain the population of the bound state at any given time. When $t = t_{fin}$, the population of the bound state at the end of the laser is obtained,

$$p_{n,l}(t) = |\langle\psi_{n,l}(\mathbf{p}) \mid \Phi(\mathbf{p},t)\rangle|^2. \quad (13)$$

III. RESULTS AND DISCUSSION

In the frequency domain, a phase-modulated laser pulse can be changed by the phase function. The chosen phase function is given by $\varphi(\omega) = A\sin[(\omega - \omega_{ref})T + \varphi_{int}]$, where ω_{ref} is the reference frequency, parameter A can modulate the amplitude of the function to change the number of subpulses in the laser pulse, parameter T can modulate the frequency of the oscillating function to alter the spacing between adjacent subpulses in the laser pulse, and parameter φ_{int} can modulate the phase offset of the sinusoidal function to change the phase difference between subpulses in the laser pulse. By varying the values of these three parameters, different shaped pulses can be obtained.

In this paper, ω_{ref} and φ_{int} are set to 0. The corresponding shaped time-domain electric-field pulse contains a series of subpulses, whose relative peak amplitude of the electric field is controlled by the value of A. Figures 1(a)–1(c), respectively, show the sinusoidally phase-modulated laser pulses for $A = 0$, 1, and 2. It can be noticed from the figure that for $A = 0$, which corresponds to the Fourier-limit pulse, there is only one central subpulse. For $A = 2$, the pulse is mainly divided into seven subpulses labeled as SP_1, SP_2, SP_3, SP_4, SP_5, SP_6, and SP_7.The intensity of the central subpulse SP_4 becomes weaker and the corresponding other subpulses SP_1, SP_2, SP_3, SP_5, SP_6, and SP_7 become stronger as A is increased.

In the following, we systematically studied the variation of the photoelectron emission spectrum of hydrogen atoms with the value of A, as shown in Fig. 2. As can be seen from the figure, the photoelectron emission spectrum has a variety of peak structures with different characteristics. As A increases, the energy of the photoelectron peaks (e.g., at the white dashed line at marker 1) with relatively large peak intensities in the photoelectron emission spectrum moves to

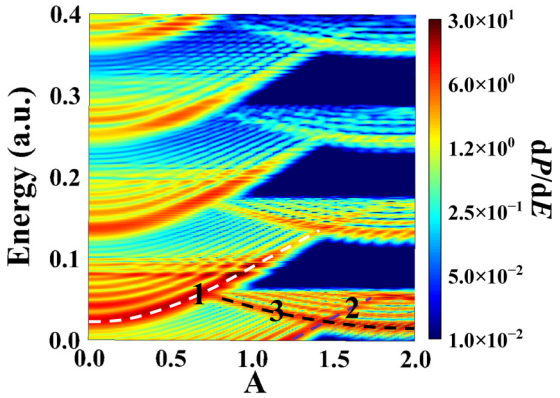

FIG. 2. Variation of the photoelectron emission spectra of hydrogen atoms under sinusoidally phase-modulated laser pulses with the value of the shaping parameter A.

higher energies, and the peak intensities gradually decrease. When the value of A is between 1.2 and 1.7, it also appears that the energy of the photoelectron peak (at the purple dashed line of marker 2) gradually shifts to higher energy with increasing A, and the peak intensity gradually decreases. When the value of A is between 0.7 and 2.0, the energy of the photoelectron peaks (at the black dashed line of marker 3) with relatively large peak intensities in the photoelectron emission spectra gradually shifts to lower energies with the increase of A, and the peak intensities gradually increase. A clear interference structure is also clearly observed. In addition to the generation of photoelectron peaks, sideband peaks are also observed to be generated next to the photoelectron peaks. The source of sideband peak generation can be attributed to the pulse width effect of the laser pulse. It is worth noting that there exist some subpeaks whose energy positions do not vary with the A value (e.g., near the energy 0.08); the corresponding photoelectron emission spectral intensities show an oscillatory behavior with the increase of the A value and still have high intensities at larger A values (e.g., $A = 0.75$), which are even stronger than the intensities of the ATI peaks.

To understand the significant differences in the photoelectron emission spectra at different A values, we analyzed the photoelectron emission process in detail. First, only the center subpulse SP_4 in Fig. 1(c) is retained in our simulation, and the electric-field peak amplitude of the other subpulses is set to 0. The photoelectron emission spectra of only the remaining SP_4 subpulse alone are calculated, as shown in Fig. 3(a). The peak amplitude of the center subpulse SP_4 is modulated by changing the shaping parameter A, as shown in Fig. 3(c). From the figure, it can be found that with the increase of the A value, the photoelectron peaks with a relatively stronger intensity in the photoelectron emission spectrum (e.g., the white dashed line at marker 1) gradually move to higher energies. The change in the photoelectron peak energy with the A value is due to the gradual decrease in the electric-field peak amplitude of the center subpulse SP_4. The white dashed line at marker 1 and the purple dashed line at marker 2 are the peak positions calculated according to the energy position equation $E_k = n\omega_0 - I_p - U_p$, which can be found to be consistent with the energy positions of the photoelectron peaks in the figure. The photoelectron peak at the white dashed line of marker 1 is

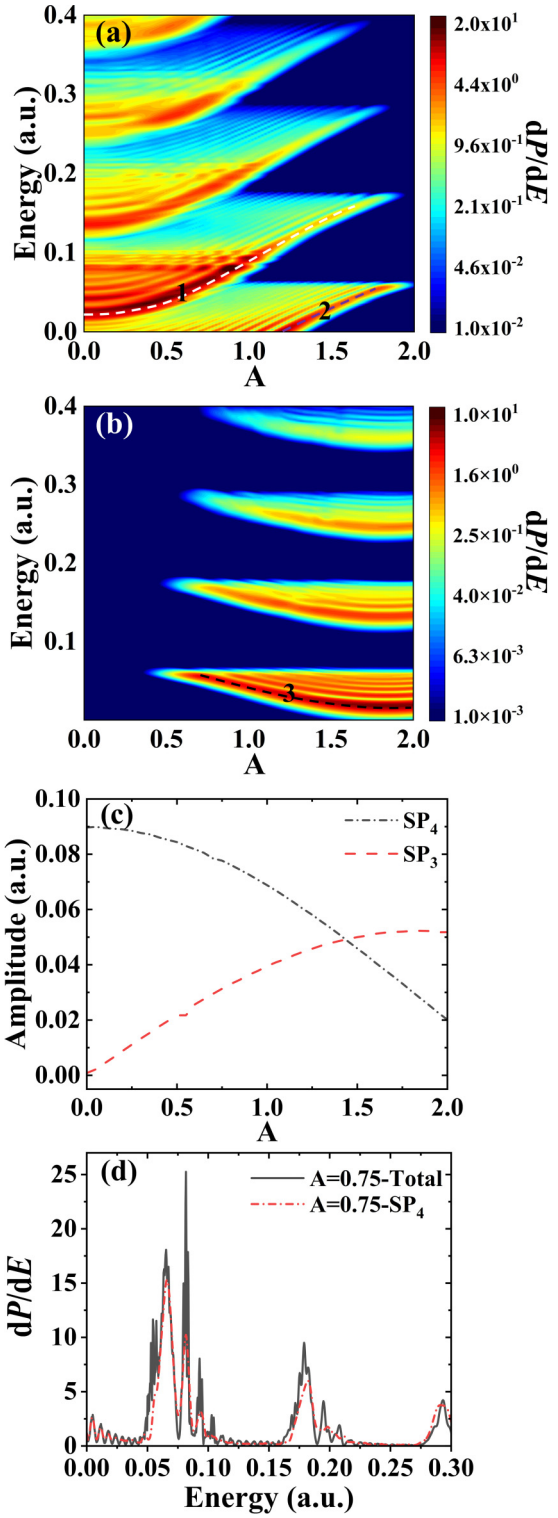

FIG. 3. (a) Variation of the photoelectron emission spectra of the hydrogen atom with the shaping parameter A under the action of only the center subpulse SP_4 in Fig. 1(c). (b) Change of the photoelectron emission spectra of the hydrogen atom with shaping parameter A in Fig. 1(c) under the effect of only the subpulse SP_3. (c) Dependence of the electric-field peak amplitude of the center subpulse SP_4 and subpulse SP_3 with the value of the shaping parameter A. (d) Photoelectron emission spectrum containing the action of all subpulses and the photoelectron emission spectrum under the action of only the central subpulse SP_4 at $A = 0.75$.

generated by the ionization of six photons, and the photoelectron peak at the purple dashed line of marker 2 corresponds to the ionization of five photons. It can also be seen that the photoelectron peak at marker 1 has a subpeak next to it, and the energy position of this subpeak moves to higher energy with the increase of the A value. Therefore, the photoelectron spectrum of Fig. 3(a) is in perfect agreement with the features of markers 1 and 2 in Fig. 2, i.e., these ionized electrons originate from the ionization of the center subpulse SP_4, and the shift of the energy position to the high-energy direction is caused by the weakening of the intensity of this subpulse with the increase of A. It is worth noting that there are some subpeaks in the range of 0–1 of A whose energy positions do not change with the value of A [e.g., the structure of the subpeak at the energy of 0.08 in Fig. 3(a)], and their peak intensities show an oscillatory behavior with the change of the A value.

Next, we further chose to retain only subpulse SP_3 and set the electric-field peak amplitude of the other subpulses to 0 to calculate the photoelectron emission spectrum, as shown in Fig. 3(b). The shaping parameter A is varied to modulate the peak amplitude of the subpulse SP_3, as presented in Fig. 3(c). From the figure, it can be found that as the value of A increases, the photoelectron peaks with a relatively stronger intensity in the photoelectron emission spectrum (e.g., the black dashed line at marker 3) gradually move to lower energies, and the peak intensity is gradually enhanced and sidebands with smaller intensities appear. The change in the energy of the photoelectron peak for the black dashed line at marker 3 with the value of A is due to the gradual increase in the intensity of the subpulse SP_3. The black dashed line at marker 3 is the peak position calculated from the energy position equation $E_k = n\omega_0 - I_p - U_p$, which is consistent with the energy position of the photoelectron peaks in the figure. The photoelectron peak for the black dashed line at marker 3 is a five-photon ionization process. This result is consistent with the behavior of the spectral peak of marker 3 in Fig. 2, indicating that the photoelectron is generated by the ionization of the ground-state electron directly absorbing five photons under the action of SP_3 (or SP_5). It is worth noting that the interference structure shown as the black dashed line of marker 3 in Fig. 2 is not found.

For considering only the center subpulse SP_4 and ignoring the effect of other subpulses, one can notice that the intensity of the peak near the energy 0.08 is weaker than that from multiple subpulses, as shown in Fig. 3(d). It indicates that multiple subpulses can modulate the excited state to enhance the intensity of the peak near the energy 0.08.

To analyze the behavior of the subpeak at the energy 0.08 in the photoelectron emission spectrum, we first calculated populations of the 2 s, 2 p, 3 s, 3 p, 3 d, 4 s, 4 p, 4 d, 4 f, 5 s, 5 p, 5 d, 5 f, and 5 g states of the atom as a function of the shaping parameter A after the laser ended, shown in Fig. 4(a). From the figure, it can be seen that the population of the 4 f state is relatively large compared to other states. As A varies, it exhibits an oscillatory characteristic, and when A is around 1, the population of the 4 f state decreases rapidly to zero. Therefore, the subpeak at the energy 0.08 is likely mainly due to the excitation of the 4 f state. In other words, under the action of a laser pulse with a frequency of 0.114,

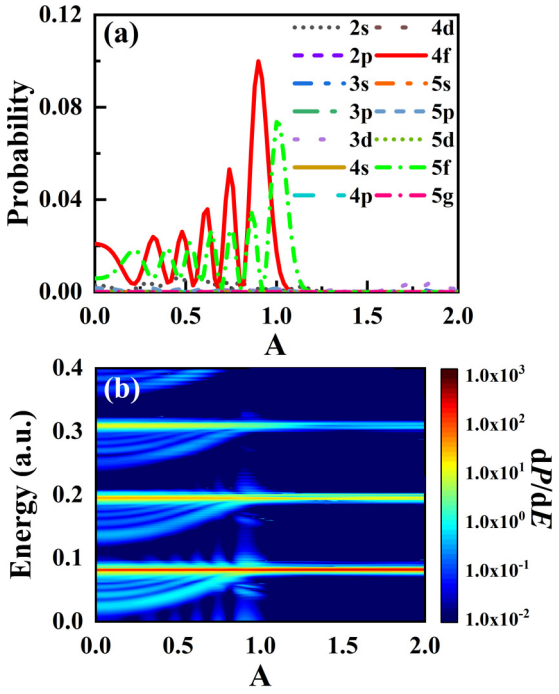

FIG. 4. (a) Variation of population in the excited state of the hydrogen atom with the value of A. (b) Change of the photoelectron emission spectrum with the A when the atomic initial state is a 4 f state.

ground-state electrons absorb four photons with the same spin angular momentum and one photon with the opposite spin angular momentum to excite to the 4 f state. Meanwhile, based on the energy conservation, due to the ac-Stark effect of the laser electric field, the higher excited state energy level shifts significantly, which allows ground-state electrons to absorb five photons to resonantly transition to the 4 f state, thereby increasing its population. Then, the electrons in the excited state 4 f are ionized.

To quantitatively confirm the contribution of the excited state, we calculated the variation of the photoelectron emission spectrum for the atom's initial state as the 4 f state with the shaping parameter A , as shown in Fig. 4(b). From the figure, it can be observed that the photoelectron emission peak at the energy 0.08 coincides with the energy position of the subpeak at the energy 0.08 on the photoelectron spectrum in Fig. 2. Therefore, the oscillating peak in the photoelectron emission spectrum can be attributed to the ground-state electrons resonantly jumping to the excited state 4 f and then directly ionizing from the 4 f state. It should be noted here that when the initial state is the 4 f state, the photoelectron emission peak does not show an oscillatory behavior with the change of the shaping parameter A. However, there is an overlap in energy between the resonance peak generated by direct ionization from the 4 f state and the subpeak generated by the laser envelope effect, which leads to a larger photoelectron emission intensity at the energy overlap between the two cases and a smaller one at the nonoverlapping range, which is characterized by an oscillation.

In order to gain a deeper understanding of the interference structure generated by the photoelectron emission spectrum in Fig. 2 (e.g., the black dashed line of marker 3), the

photoelectron emission process produced by the joint action of multiple subpulses was analyzed. Here, the change of the photoelectron emission spectra with the value of A is simulated when only the subpulses SP_1, SP_2, SP_3, and SP_4 act with the hydrogen atom, as shown in Fig. 5(a). It can be noticed from the figure that there is no interference structure evident at the position of the black dashed line at marker 3 in Fig. 2 [inside the black dashed box in Fig. 5(a)]. We proceeded to simulate the variation of the photoelectron emission spectrum with the value of A by only subpulses SP_1, SP_2, SP_3, SP_4, and SP_5, as exhibited in Fig. 5(b). From the figure, it can be observed that the emission peaks in the photoelectron spectrum [inside the black dashed box in Fig. 5(b)] appear with the same complex interference structure as that at the black dashed line of marker 3 in Fig. 2. Therefore, the generation of the interference structure in the photoelectron emission spectrum may be related to the interference of those ionized electrons from the subpulses SP_1, SP_2, SP_3, SP_4, and SP_5. To further find the reason for the generation of the interference structure, we calculated the photoelectron emission spectrum generated from only SP_3, SP_4, and SP_5, as shown in Fig. 5(c). From the figure, it can be found that the generated interference structure in the photoelectron emission spectrum [inside the black dashed box in Fig. 5(c)] is almost the same as that in Fig. 5(b).

We also gave the photoelectron emission spectra of the subpulses SP_3, SP_4, and SP_5 at $A = 2$ (red dashed line) versus the spectra from all subpulses (black line), as shown in Fig. 5(d). The inset shows an enlarged view of the energy range 0.01–0.22. From the figure, it can be found that the photoelectron emission spectrum generated from only subpulses SP_3, SP_4, and SP_5 (red dashed line) is characterized by a clear interference, and the depth of the interference modulation is a little weaker than that of the modulation of all subpulses. Because the energy position of the photoelectron peak produced by the center subpulse SP_4 is inconsistent with that in the black dashed box, the interference structure in the photoelectron emission spectrum is generated mainly by the interference between the ionized electrons from subpulses SP_3 and SP_5.

To understand the effect of the pulse shaping on ionization and excitation, the time-dependent population of the excited state was studied. Figure 6(a) gives the laser electric field for a laser pulse $A = 0.75$ with the sinusoidal phase modulation. It can be seen that the subpulse with the stronger intensity in this pulse is SP_4. Figure 6(b) presents the change of the excited state population with time calculated for the sinusoidal phase-modulation laser pulse $A = 0.75$. It can be noticed from the figure that the excited state population is 0.15 at $t = 330$ o.c., while it decreases significantly to 0.12 at $t = 396$ o.c. The rapid decrease in its population is mainly due to the action of the subpulse SP_5. In order to gain insight into the role of subpulse SP_5, we calculated the photoelectron emission spectra at the moments $t = 330$ and $t = 396$ o.c. in the case of $A = 0.75$, as shown in Fig. 6(c). From the figure, it can be found that the peak intensities of the photoelectron emission spectra calculated at $t = 330$ and $t = 396$ o.c. moments at the photoelectron peak with energy of 0.06 are the consistent ones. However, the intensity of the resonance peak at the electron energy of 0.08 in the photoemission spectrum at $t = 396$

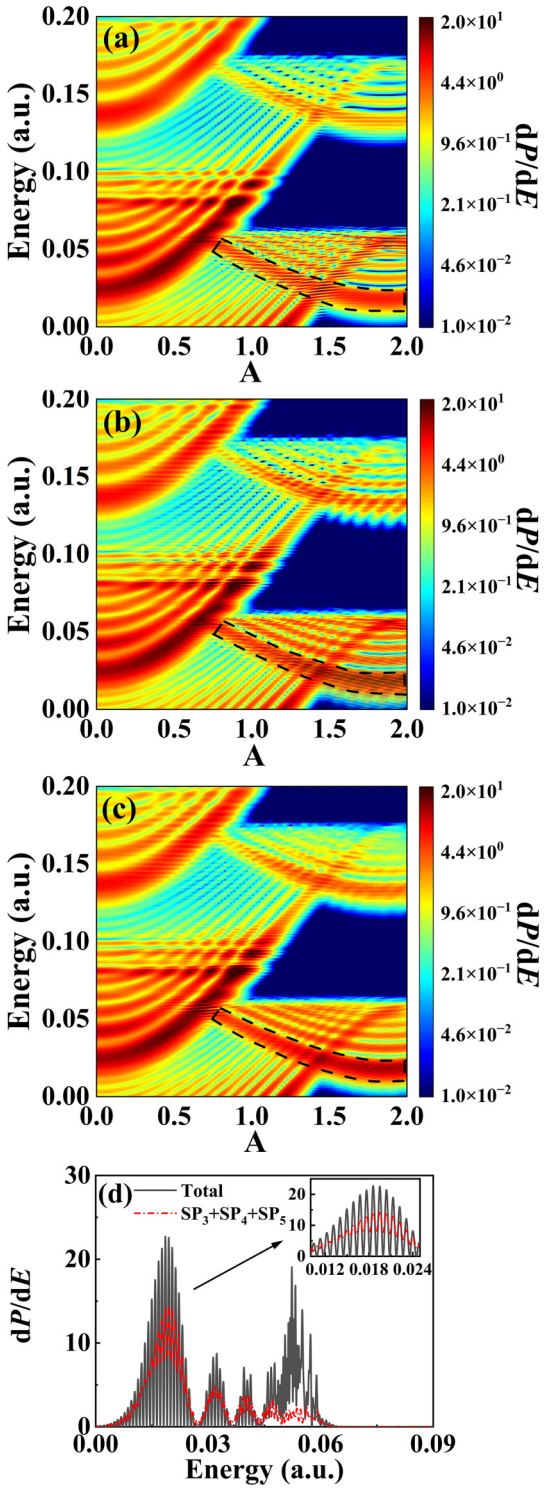

FIG. 5. (a) Variation of the photoelectron emission spectra of hydrogen atoms under the effect of subpulses SP_1, SP_2, SP_3, and SP_4 with the change of shaping parameter A in Fig. 1(c). (b) Dependence of the photoelectron emission spectra of hydrogen atoms under the effect of subpulses SP_1, SP_2, SP_3, SP_4, and SP_5 with the change of shaping parameter A in Fig. 1(c). (c) Variation of the photoelectron emission spectra of hydrogen atoms under the effect of subpulses SP_3, SP_4, and SP_5 with the change of shaping parameter A in Fig. 1(c). (d) Photoelectron emission spectra produced by only subpulses SP_3, SP_4 with SP_5 (red dashed line), and all subpulses (black line) at $A = 2$.

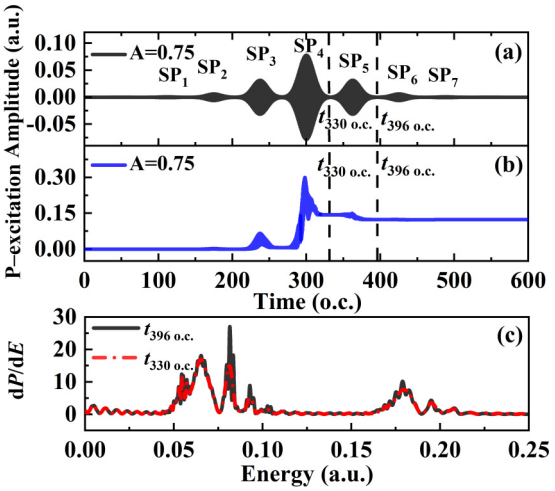

FIG. 6. (a) Laser pulse with sinusoidal phase modulation at $A = 0.75$. (b) Excited state population at $A = 0.75$ as a function of time. (c) Photoelectron emission spectra at different moments under $A = 0.75$.

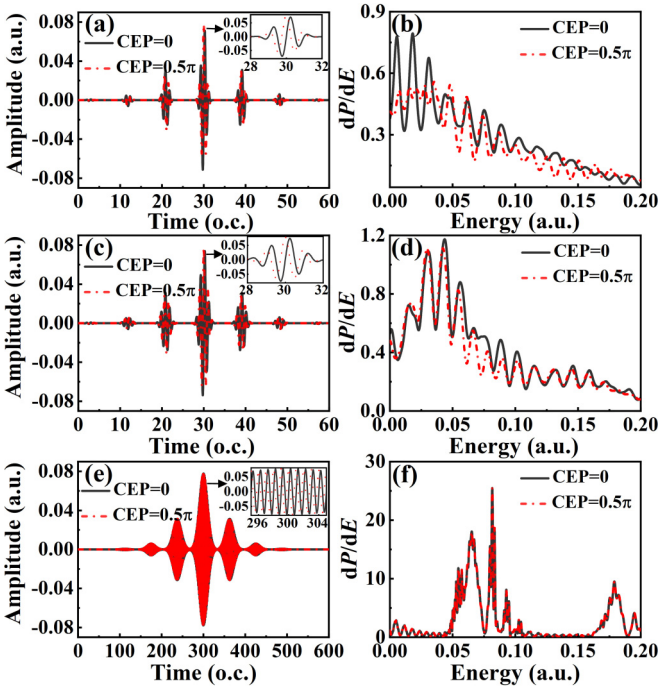

FIG. 7. (a) Sinusoidal phase-modulated laser pulse at $A = 0.75$ for a pulse width of 1.8 fs before shaping, and (b) photoelectron emission spectra at $A = 0.75$ with the CEP of 0 and 0.5π, respectively. (c) Sinusoidal phase-modulated laser pulse at $A = 0.75$ with a pulse width of 2.4 fs before shaping, and (d) photoelectron emission spectra from 2.4 fs sinusoidal phase-modulated laser pulses at $A = 0.75$ with the CEP of 0 and 0.5π, respectively. (e) Sinusoidal phase-modulated laser pulse at $A = 0.75$ for a pulse width of 31.2 fs before shaping, and (f) photoelectron emission spectra from 31.2 fs sinusoidal phase-modulated laser pulses at $A = 0.75$ with the CEP of 0 and 0.5π, respectively.

o.c. is significantly greater than that in the photoemission spectrum at $t = 330$ o.c. It can be seen that the subpulse SP_5 modulates the population of the excited state and ionization occurs from this state, which enhances the intensity of the resonance peak at energy 0.08. Therefore, when the total energy of the pulse is constant, the time-domain behavior of the pulse can be modulated by shaping the pulse, and the behavior of ionization and excitation of atoms can be controlled by changing different shaping parameters.

We further investigated the effect of CEP on the photoelectron emission spectrum of the shaping pulse. Figures 7(a), 7(c), and 7(e) present sinusoidal phase-modulated laser pulses at $A = 0.75$ for pulse widths of 1.8, 2.4, and 31.2 fs before shaping, respectively. The corresponding photoelectron emission spectra at CEP $= 0$ and CEP $= 0.5\pi$ are shown in Figs. 7(b), 7(d), and 7(f), respectively. From Fig. 7(b), it can be found that there is a significant difference between the photoelectron emission spectra produced by CEP $= 0$ and CEP $= 0.5\pi$ when the pulse width of the laser pulse before shaping is 1.8 fs. When the pulse width of the sinusoidal phase-modulation laser pulse is 2.4 fs, the photoelectron emission spectra produced by CEP $= 0$ and CEP $= 0.5\pi$ are not much different, and some of the peaks are completely coincident, as displayed in Fig. 7(d). In contrast, the photoelectron emission spectra produced by CEP $= 0$ and CEP $= 0.5\pi$ are identical for the pulse width of 31.2 fs for the laser pulses before shaping, as exhibited in Fig. 7(f). Therefore, for the shaping pulse case, the peak positions in the photoelectron emission spectra are significantly different for changing the CEP for laser pulses with a relatively short duration, but the photoelectron emission spectra have no effect at all for varying the CEP for laser pulses with a relatively long duration.

IV. CONCLUSIONS

In summary, by solving the time-dependent Schrödinger equation in momentum space, we investigated the photoelectron emission from atoms irradiated by sinusoidal phase-modulated shaping pulses. It was demonstrated that by controlling the phase amplitude of the pulse in the frequency domain, the excitation and ionization of atoms can be modulated, and thus the results of this modulation are manifested in the photoelectron emission spectrum. In addition to the ATI peak, additional resonance peaks and interference structures can be observed in the photoelectron emission spectra. This study indicates that the shaped pulse can be applied to control the photoelectron emission.

ACKNOWLEDGMENTS

This work was supported by the National Key Research and Development Program of China (Grant No. 2019YFA0307700), National Natural Science Foundation of China (Grants No. 12074145, No. 11975012, No. 11774129, and No. 12374029), the Outstanding Youth Project of Taizhou University (Grant No. 2019JQ002), and the Jilin Provincial Research Foundation for Basic Research, China (Grant No. 20220101003JC). The authors acknowledge the High Performance Computing Center of Jilin University for supercomputer time and the high-performance computing cluster Tiger@ IAMP.

[1] P. Kruit, J. Kimman, and M. J. Van der Wiel, J. Phys. B **14**, L597 (1981).

[2] G. Petite, F. Fabre, P. Agostini, M. Crance, and M. Aymar, Phys. Rev. A **29**, 2677 (1984).

[3] R. R. Freeman, P. H. Bucksbaum, H. Milchberg, S. Darack, D. Schumacher, and M. E. Geusic, Phys. Rev. Lett. **59**, 1092 (1987).

[4] P. Agostini, F. Fabre, G. Mainfray, G. Petite, and N. K. Rahman, Phys. Rev. Lett. **42**, 1127 (1979).

[5] N. Suárez, A. Chacón, M. F. Ciappina, B. Wolter, J. Biegert, and M. Lewenstein, Phys. Rev. A **94**, 043423 (2016).

[6] N. Suárez, A. Chacón, E. Pisanty, L. Ortmann, A. S. Landsman, A. Picón, J. Biegert, M. Lewenstein, and M. F. Ciappina, Phys. Rev. A **97**, 033415 (2018).

[7] X.-F. Li, Y. Qiao, D. Wu, R.-X. Yu, J.-G. Chen, J. Wang, F.-M. Guo, and Y.-J. Yang, Chin. Phys. B **33**, 013302 (2023).

[8] Y. Qiao, J. Chen, Y. Huo, H. Liang, R. Yu, J. Chen, W. Liu, S. Jiang, and Y. Yang, Phys. Rev. A **107**, 023523 (2023).

[9] Y.-J. Yang, J.-G. Chen, F.-P. Chi, Q.-R. Zhu, H.-X. Zhang, and J.-Z. Sun, Chin. Phys. Lett. **24**, 1537 (2007).

[10] Y. Qiao, Y. Huo, H. Liang, J. Chen, W. Liu, Y. Yang, and S. Jiang, Phys. Rev. B **107**, 075201 (2023).

[11] K. M. Dorney, T. Fan, Q. L. D. Nguyen, J. L. Ellis, D. D. Hickstein, N. Brooks, D. Zusin, C. Gentry, C. Hernández-García, H. C. Kapteyn *et al.*, Opt. Express **29**, 38119 (2021).

[12] Y. Qiao, J. Chen, S. Zhou, J. Chen, S. Jiang, and Y. Yang, Chin. Phys. Lett. **41**, 014205 (2024).

[13] P. Agostini and L. F. DiMauro, Adv. At. Mol. Opt. Phys. **61**, 117 (2012).

[14] D. B. Milošević, G. G. Paulus, and W. Becker, Opt. Express **11**, 1418 (2003).

[15] X. M. Tong, K. Hino, and N. Toshima, Phys. Rev. A **74**, 031405(R) (2006).

[16] G. Lagmago Kamta and A. D. Bandrauk, Phys. Rev. A **74**, 033415 (2006).

[17] M. Meckel, D. Comtois, D. Zeidler, A. Staudte, D. Pavičić, H. C. Bandulet, H. Pépin, J. C. Kieffer, R. Dörner, D. M. Villeneuve *et al.*, Science **320**, 1478 (2008).

[18] P. V. Demekhin and L. S. Cederbaum, Phys. Rev. A **88**, 043414 (2013).

[19] C. Yu, N. Fu, G. Zhang, and J. Yao, Phys. Rev. A **87**, 043405 (2013).

[20] C. Yu, N. Fu, T. Hu, G. Zhang, and J. Yao, Phys. Rev. A **88**, 043408 (2013).

[21] M. Goto and K. Hansen, Chem. Phys. Lett. **522**, 23 (2012).

[22] A. Monmayrant, S. Weber, and B. Chatel, J. Phys. B: At. Mol. Opt. Phys. **43**, 103001 (2010).

[23] D. Brinks, R. Hildner, F. D. Stefani, and N. F. van Hulst, Opt. Express **19**, 26486 (2011).

[24] A. Präkelt, M. Wollenhaupt, C. Sarpe-Tudoran, and T. Baumert, Phys. Rev. A **70**, 063407 (2004).

[25] M. Wollenhaupt, A. Präkelt, C. Sarpe-Tudoran, D. Liese, T. Bayer, and T. Baumert, Phys. Rev. A **73**, 063409 (2006).

[26] J. Lahiri, S. H. Yuwono, I. Magoulas, M. Moemeni, B. Borhan, G. J. Blanchard, P. Piecuch, and M. Dantus, J. Phys. Chem. A **125**, 7534 (2021).

[27] S. Li, B. Jochim, J. Stamm, D. Peng, H.-C. Shao, J. M. Ngoko Djiokap, and M. Dantus, Phys. Rev. A **105**, 053105 (2022).

[28] H.-Y. Yuan, F.-M. Guo, D.-Y. Zhang, J. Wang, J.-G. Chen, and Y.-J. Yang, Chin. Phys. B **27**, 103201 (2018).

[29] Z.-Z. Zhou and S.-I. Chu, Phys. Rev. A **83**, 013405 (2011).

[30] H. Yuan, Y. Yang, F. Guo, J. Wang, and Z. Cui, Opt. Express **30**, 19745 (2022).

[31] H. Yuan, Y. Yang, F. Guo, J. Wang, J. Chen, W. Feng, and Z. Cui, Opt. Express **31**, 24213 (2023).

[32] R. H. Landau, Phys. Rev. C **27**, 2191 (1983).

[33] K. M. Maung, D. E. Kahana, and J. W. Norbury, Phys. Rev. D **47**, 1182 (1993).

[34] J. W. Norbury, K. M. Maung, and D. E. Kahana, Phys. Rev. A **50**, 2075 (1994).

[35] Y. Rae Kwon and F. Tabakin, Phys. Rev. C **18**, 932 (1978).